

**ROTOR SIZE OPTIMISATION OF A
COUNTER ROTATING DUAL ROTOR
WIND TURBINE****ELLENIRÁNYÚ IKERSZÉLTURBINÁK
ROTORMÉRETEINEK VIZSGÁLATA**HETYEI Csaba¹ – SZLIVKA Ferenc²**Abstract**

The customers growing demand for energy utilization and the need for green and sustainable energy have changed our energy security. Changes in the energy mix have become necessary by the developments and improvements of the energy producers and the need by the population for an energy-efficient and sustainable future, thus today's expectation in this engineering field is to design more efficiently and sustainably than ever before in an economically efficient way. In our article, we are reviewing the conventional and the newly spreading non-conventional wind turbines and their place of use. After this overview, we are presenting the foundation of wind turbines efficiency and its power coefficient. Later, we are introducing a Computational Fluid Dynamics (CFD) simulation for a Counter-Rotating Dual-Rotor Wind Turbine (CO-DRWT) with different rotor sizes. After the simulation, we are examining the overall power coefficient of turbines and its change by the turbine size.

Keywords

CO-DRWT, CFD, Dual-Rotor Wind Turbine, Twin turbine, Simulation

Absztrakt

Energiabiztonságot nagyban befolyásolja a fogyasztó oldali növekvő energiafelhasználás és a felhasználói oldalról a termelők felé érkező zöld energia igénye. Az energiamixbeli változások szükségessé tették energiatermelő gépjeink fejlesztését és módosítását, melynek célja a jobb hatásfok, a fenntartható és környezetbarát üzem a lehetőségekhez mérten költséghatékonyan. Cikkünkben áttekintjük a hagyományos és a napjainkban elterjedő nem hagyományos szélturbinák típusait és felhasználásuk helyszíneit. Ezt követően ismertetjük a szélturbinák teljesítménytényezőjének kiszámítási módját. Ezután végestérfogat alapú áramlástanai szimulációval ellenirányú ikerturbinák energiatermelését vizsgáljuk eltérő rotorméretekkel. Cikkünk zárásaként meghatározzuk a két turbina teljesítménytényezőjét az átmérőváltozás függvényében.

Kulcsszavak

CO-DRWT, CFD, Kétturbinás turbina, Iker-turbina, Szimuláció

¹ hetyei.csaba@uni-obuda.hu | ORCID: 0000-0003-2915-4540 | PhD student/doktorandusz | Óbudai Egyetem Biztonságtudományi Doktori Iskola

² szlivka.ferenc@bgk.uni-obuda.hu | ORCID: 0000-0002-3298-4142 | Professor/egyetemi tanár | Óbudai Egyetem Bánki Donát Gépész és Biztonságtechnikai Mérnöki Kar

INTRODUCTION

Wind energy is one of the most popular renewable energy sources. At the beginning of the civilization the humans have used for sailing, and then for milling. The first known sketch from a windmill was made by Heron of Alexander in the first century. The first known windmill was found in Great Iran near Nashtifan, which was used for flour grinding. By the archaeological research, the Nashtifan Windmills was built in the 9th century, three centuries earlier than the first known windmills in north-western Europe [1]. The Nashtifan Windmill was a vertical axis windmill, which is shown in Figure 1.

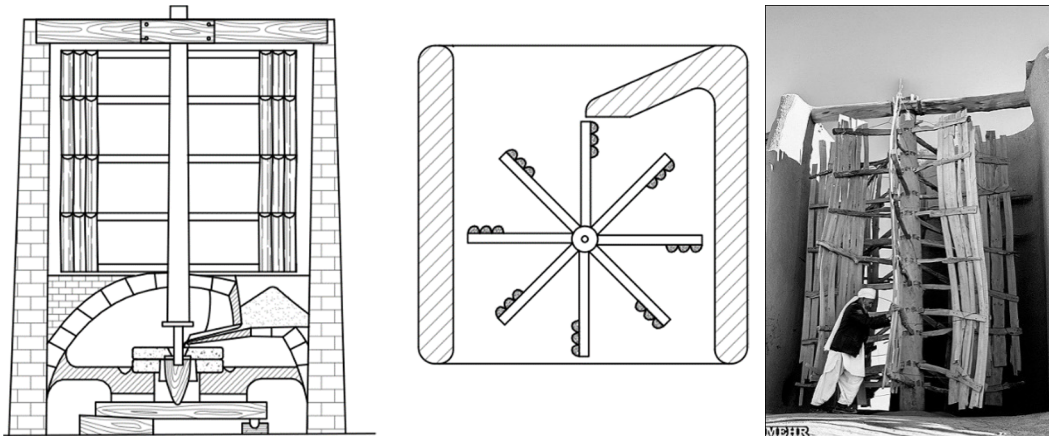


Figure 1. Conceptual outline and reconstructed version of Nashtifan Windmill [2]

In Europe, the horizontal axis windmill was popular. This kind of windmill nowadays known than the “Dutch windmill”. The horizontal axis windmill illustration from Miles Kelly shown in Figure 2.



Figure 2. Miles Kelly's Cross-Section of Wooden Windmill [3]

In the middle of the 19th century, the American Windmill was invented by Daniel Halladay. This windmill was used generally for lifting water. After three decades of the invention of the American Windmill, the first vertical axis wind turbine (VAWT) was invented in 1887 by James Blyth and the first horizontal axis wind turbine (HAWT) was invented in 1888 by Charles Brush [4].

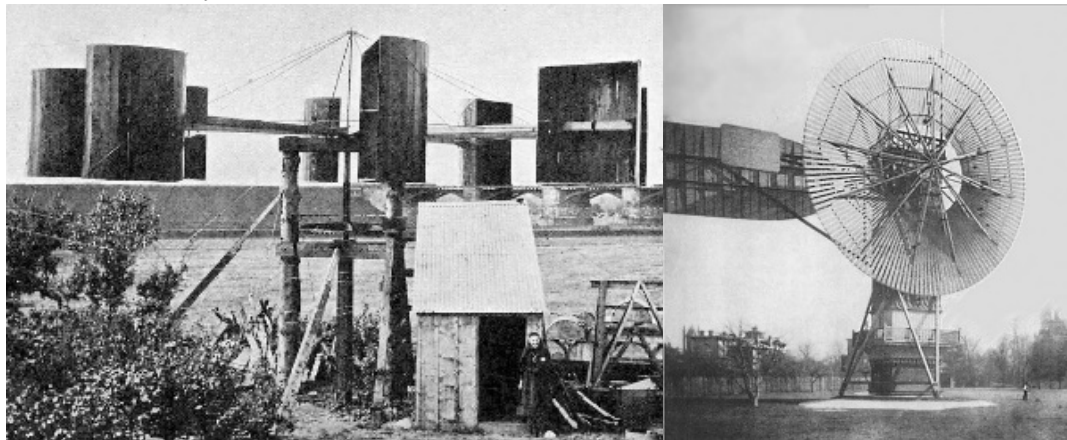


Figure 3. James Blyth's VAWT (left) and Charles F. Brush's HAWT (right) [5, 6]

After the first wind turbines, the wind energy than a source of the electricity started spreading and evolving. Example in Yalta in 1931, the first 100 kW wind turbine was built, which has 8.5 times wmore capacity than Charles F. Brush's wind turbine.

After the 70's, 80's oil crisis the renewable energy sources (including the wind energy) became more and more into the focus, and it speeds up the innovation of the wind turbines. Nowadays fear from the nuclear accident and the environmental damage, the wind turbine installation progressively starts growing. This process can be seen in the global statistics, for example in BP's 2019 report [7] which can see in the next figure.

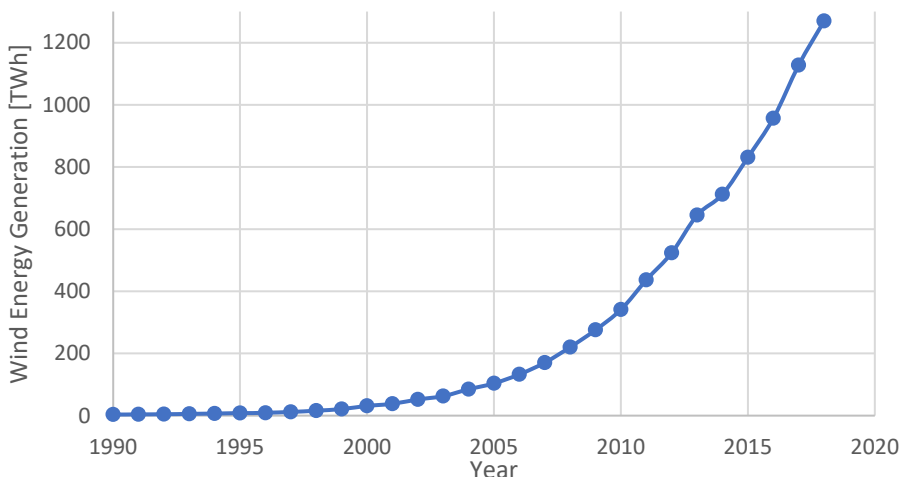


Figure 4. Wind energy generation globally by year in Terawatt-hour [7]

This growing trend can be observed for the small-scale turbines among the medium and large-scale turbines. According to the Canadian Wind Energy Association [8], the small size turbines have 1-30 kW capacity and typically mounted on 24-43 m high tower. Thanks, this small size and scalability the wind turbines can be installed in the urban areas, where the required energy need is higher and the spaces are limited. The small-scale wind turbines with a proper SCADA (Supervisory Control and Data Acquisition) system can play an important role in the smart cities. Three possible use of wind turbines can be seen in Figure 5.



*Figure 5. Wind turbines in urban regions:
a, Roof-mounted WTs [9]; b, Mini wind turbine and solar cell on a street light pole in Budapest [10];
c, VAWT and solar panel between passing vehicles in Istanbul [11]*

In limited spaces, example the previously mentioned urban areas, choosing the right wind turbine is a difficult job, because the wind speed and direction can be altered quickly, or the wind turbine's noise can disturb the residents. For the different requirements and use the engineers must design different wind turbines. These newly designed wind turbines called unconventional wind turbines. Each unconventional wind turbine has a different feature than the others, which makes the products installable in the desired zone.

In Figure 6 there are three different unconventional wind turbines. In Figure 6./a there is a multiple rotor wind turbine, where on the same tower there are two or more rotors. In the picture, there is just two-rotor and they have different rotational direction, therefore these we call this type to counter-rotating dual-rotor wind turbine (CO-DRWT). When the rotors are not mirrored, and they have the same rotational direction they are the co-rotational

dual-rotor wind turbines (CR-DRWT). In Figure 6/b, there is a conventional wind turbine extended with a guide baffle. This external narrowing wind tunnel can increase the kinetic energy of the wind. In Figure 6/c, there is the Archimedes Screw Wind Turbine, which can operate with low noise as a result of its relatively low rotational speed.



Figure 6. Unconventional WTs a, Dual-Rotor Wind Turbine [12]; b, Wind turbine with guide baffle [13]; c, Archimedes Screw Wind Turbine [14]

Ozbay *et al.* [15] have a measurement with the previously mentioned the counter and co-rotating dual-rotor wind turbines, where they are compared the CO and CR-DRWTs' power coefficient with a single rotating wind turbine (SRWT). They found the DRWTs can produce more electricity than an SRWT, and they are also discovering the counter-rotating dual-rotor wind turbines can harvest more energy than the CR-DRWTs.

Lee *et al.* [16] performed a simulation for a CO-DRWT's power coefficient (c_p) using the blade element momentum theory and they compared with an SRWT's c_p . The study has shown for different pitch angle, rotating speed, and radius the CO-DRWT have higher performance than the SRWT.

THE FOUNDATION OF WIND TURBINES EFFICIENCY

The WTs are complex electro-mechanical systems, which convert the available wind energy into rotational kinetic energy by their blades and then, with their generator

convert the rotational energy into electrical energy. The first and the simplest description of this procedure's first part was made by Betz in 1919.

For the definition of Betz's limit, Betz uses the principles of conservation of mass and momentum with a turbine which has infinite blades, thus the turbine is an actuator disk, hence the Betz's coefficient has no dependency on the geometry and besides, the fluid flow is incompressible, laminar, frictionless, and the force and pressure distribution on the turbine are uniform.

For the Betz's limit explanation, we have to use a flow domain, as shown in Figure 7. For the coefficient, we have to write two Bernoulli's equation for each side of the domain. The first from the inlet 1 to the turbine's front face (called e on the next figure), and the second from the turbine back face (called u on the next figure) to the outlet 2.

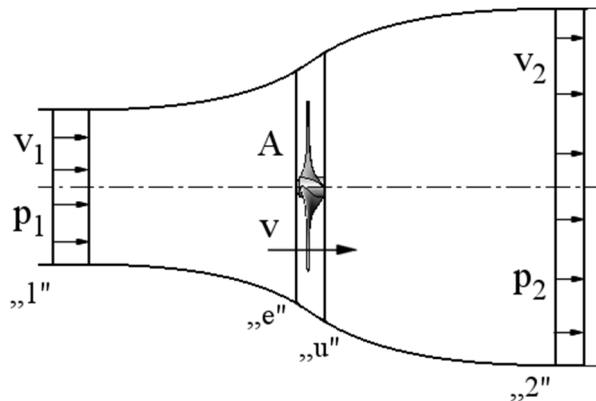


Figure 7. Computational domain for the calculation of the Betz's coefficient

If we assume the environmental pressures (p_1 and p_2) on the domain's inlet and outlet faces are equal and if we assume the velocities (v_e and v_u) also equal on the turbine's front and back faces, the sum of the two Bernoulli's equation are the equation (1).

$$p_u - p_e = \frac{1}{2} \cdot \rho \cdot (v_2^2 - v_1^2) \quad (1)$$

In the previous equation p_u is the pressure on the blade's back face, p_e is the pressure on the blade's front face, v_1 is the domain's inlet velocity, v_2 is the outlet velocity from the domain, ρ is the fluid's density. Using the continuity equation for the control volumes the mass flow rate is given by the following equation.

$$\dot{m} = \rho \cdot A_1 \cdot v_1 = \rho \cdot A \cdot v = \rho \cdot A_2 \cdot v_2 \quad (2)$$

In equation (2) the \dot{m} , is the first time derivative of the mass of the fluid, A_1 is the area of the inlet face, A is the area of the turbine swept surface, A_2 is the area of the outlet face, and v is the speed of the fluid on the A surface.

Using Newton's second law, the turbine's kinetic energy and its power equation are the following:

$$P = \dot{E} = \frac{1}{2} \cdot \rho \cdot A \cdot v_1^3 \cdot \left(\frac{1 + \frac{v_2}{v_1}}{2} \cdot \left(1 - \left(\frac{v_2}{v_1} \right)^2 \right) \right) \quad (3)$$

Differentiating the equation (3), the maximum value of P is at $v_2/v_1 = 1/3$. Substituting back this value to equation (3), the Betz's coefficient definable by the equation (4).

$$P = \frac{1}{2} \cdot \rho \cdot A \cdot v_1^3 \cdot \left(\frac{1 + \frac{1}{3}}{2} \cdot \left(1 - \left(\frac{1}{3} \right)^2 \right) \right) = \frac{1}{2} \cdot \frac{16}{27} \cdot \rho \cdot A \cdot v_1^3 \quad (4)$$

In equation (4) the $16/27$ (59.259%) is the Betz's coefficient, which is theoretically the maximum for a wind turbine's power coefficient (c_p) [1].

By the GGS [17] model, which is a curvilinear model against the rectilinear Betz model, the c_p 's maximum value is 30.113%. By measurements, the WTs' power coefficient usually between these two limits.

In a computational fluid dynamics (CFD) simulation software the c_p can be calculated with the following equation:

$$c_p = \frac{P_{rotor}}{P_{wind}} = \frac{M \cdot \omega}{\frac{1}{2} \cdot \rho \cdot A \cdot v_\infty^3} \quad (5)$$

In the previous equation, P_{rotor} is the rotor's power, P_{wind} is the wind power, M is the torque on the rotor, ω is the rotor's angular velocity, ρ is the density of the air, A is the swept area, v_∞ is the freestream velocity.

For dual-rotor wind turbines, the swept area alters depending on the second turbine position or diameter. In our cases, we used different rotor sizes with a constant radial and axial shift, these layouts are shown in Figure 8.

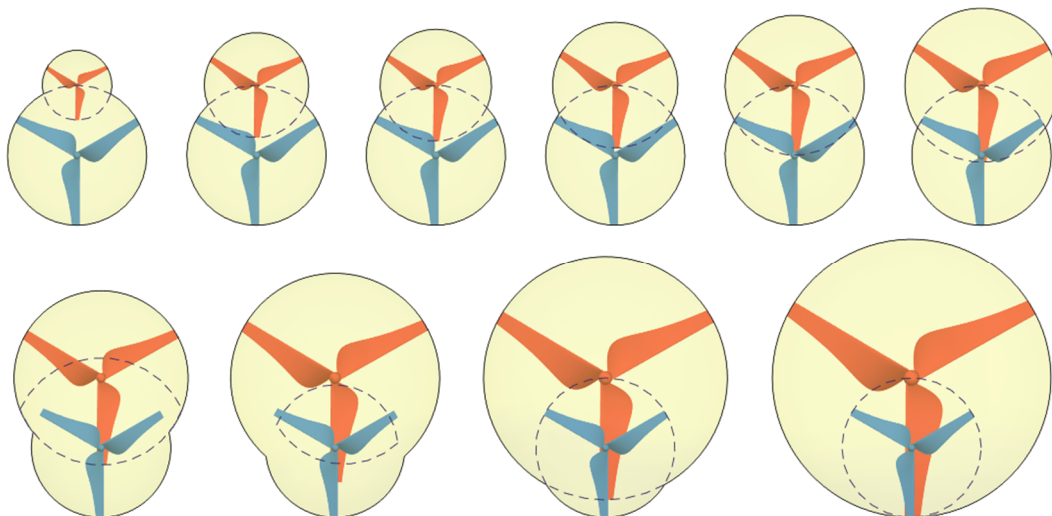


Figure 8. Swept area for different turbine diameters

FOUNDATIONS OF COMPUTATIONAL FLUID DYNAMICS

The computational fluid dynamics (CFD) simulation is a tool for imitating the physical world. For our research, we used a finite volume method (FVM) based CFD software. This method divides the computational domain into finite volumes, within it is using the continuity, momentum, and energy equations to compute the flow field's properties. Based on the three previous equations the FVM based CFD codes generally use the following transport equation [18]:

$$\frac{\partial}{\partial t} \int_V U dV + \oint_A \underline{F} d\underline{A} - \int_V S_V dV - \oint_A \underline{S}_A d\underline{A} = R \quad (6)$$

In this equation, V denotes an arbitrary enclosed control volume, A denotes the surface of this control volume, U is a conserved quantity (e.g.: mass), F is the same quantity's flux over the A surface, S_V is the volumetric source of quantity U over volume V , S_A is the surface source of quantity U over surface A , and R is the error of the equation (residual).

The previous equation can be written for every cell of the mesh and solved in a system of equations. To do so, CFD codes utilise iterative methods that converge to a solution by reducing the residuals of the equations.

MOTIVATION

In this research, with the previously described numerical method a CO-DRWT's wheel was studied, without the WT parts (e.g. nacelle, tower, interior parts). In our simulations, we choose two rotors, the first with 200 mm diameter, the second with varied sizes. The two turbines are mirrored and rotated with 180° as Figure 9 shown for the $D_2/D_1=1$ case.

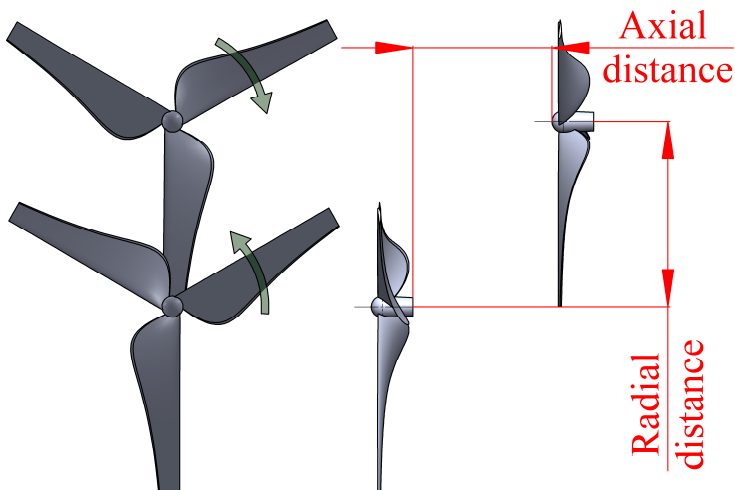


Figure 9. Studied CO-DRWT with 0.5D radial and axial shift with rotational directions indicated

For different configurations, the swept area was varying. In our cases for the areas were between 35762.24 mm² and 125663.71 mm².

For having a similar flow condition for the turbines, we choose 4 for the tip speed ratio, which is describing the relationship between the turbine's rotational speed and the wind velocity. This relationship can be determined with the following equation:

$$\lambda = \frac{\omega \cdot R}{v_{\infty}} \quad (7)$$

In the previous equation, λ is the tip speed ratio, ω is the angular velocity, R is the blade's radius, and v_{∞} is the freestream velocity.

By numerical simulation, we were able to monitor the torque values on the turbines, which was changing by the turbine size as well. For easier comparison, we have calculated the turbines overall power coefficients (c_p) by with the equation (5), and we were compared its values.

MEASUREMENT METHOD

For validation, specimens were manufactured by 3D printing. The printed version of the turbine has the same diameter and there are shown in Figure 10.



Figure 10. 3D printed turbines

The generated torque on the 3D printed rotors was determined by wind tunnel measurements [19]. The measurement setup is shown in Figure 11.



Figure 11. Wind turbine models in the wind tunnel

SIMULATION PARAMETERS

For the simulations, we used a rectangular computational domain, which is shown with the domain size and the first rotor's position in Figure 12. The second rotor's position was fixed with $0.5D$ axial and radial distance from the first rotor as it was shown previously in Figure 9.

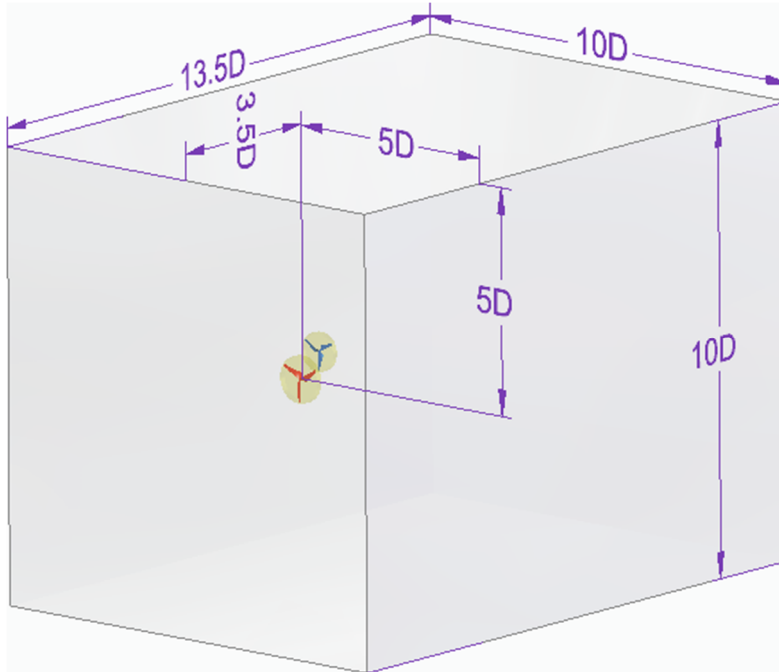


Figure 12. Computational domain

For the numerical simulations, we were employed Mentor Graphics' FLOEFD. From the CFD software material database, the „Air” was chosen as fluid. The flow enters the computation domain through its “front” face with $3.79 \text{ m}\cdot\text{s}^{-1}$ freestream velocity. For the other boundaries of the domain, an environment pressure of 1 atm was prescribed.

Each turbine's tip speed ratio was 4, according to which the first turbine's speed of rotation was 24.1279 RPS, the second turbine's angular velocity was varying between 12.0639 and 48.2558 RPS depending by the turbine's radius. The turbines' rotation was modelled with frozen rotor method.

In each simulation, the $k-\varepsilon$ turbulence model was used with a two-scale wall function based on the Van Driest model.

The simulation ran with two finishing conditions, the first was the monitored values should converge, the second was the simulation should run for 18 travels. The monitored values were the torque on each turbine. The travel is a special stopping criterion, which is the estimated iteration requirement for the information exchange between the two furthest points within the computation domain, thus 18 travels mean a virtual particle can travel 18 times over the whole computational domain. In our cases, 1 travel was between 300-350 iterations depending on the geometry and the mesh.

For the $D_2/D_1 = 1.25$ case the torque versus the iterations shown in Figure 13. In the next figure, the opposite sign indicates the different direction of rotation.

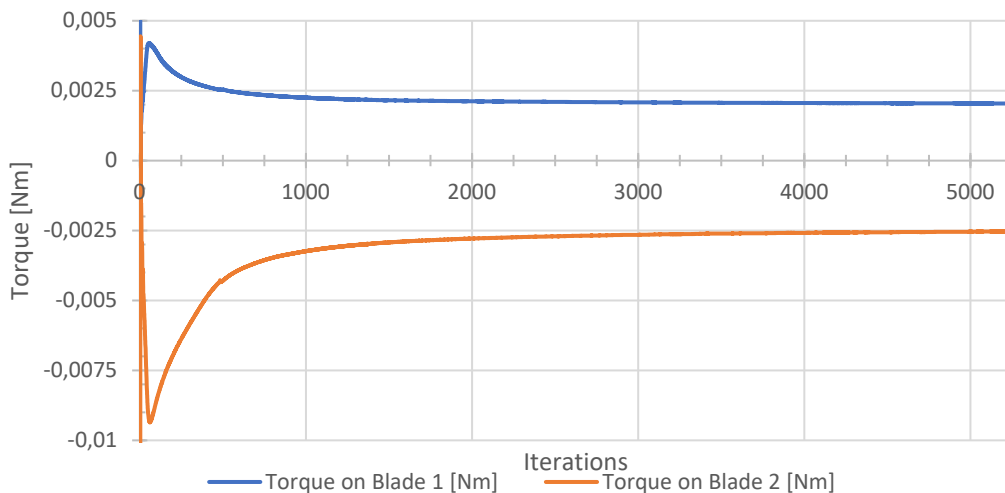


Figure 13. Torque convergence for $D_2/D_1 = 1.25$ case

The FLOEFD is a finite volume based CFD software, which provides a cartesian mesh with cell mating and cut-cell refinement methods, based on Mentor Graphics' SmartCells technology. We started each simulation with an initial grid approx. 1.5-2 million elements depending on the geometry, and with adaptive mesh refinement, the mesh was refined with the limit of 3.25 million elements. The refinements occur at 2, 5, 7, 10, 15, 16, and 17 travels.

For the $D_2/D_1 = 1.25$ case, the initial mesh had 1 656 895 elements and with adaptive remeshing, it was finer to 3 248 602 elements. The initial and the final mesh are shown in the next figure.

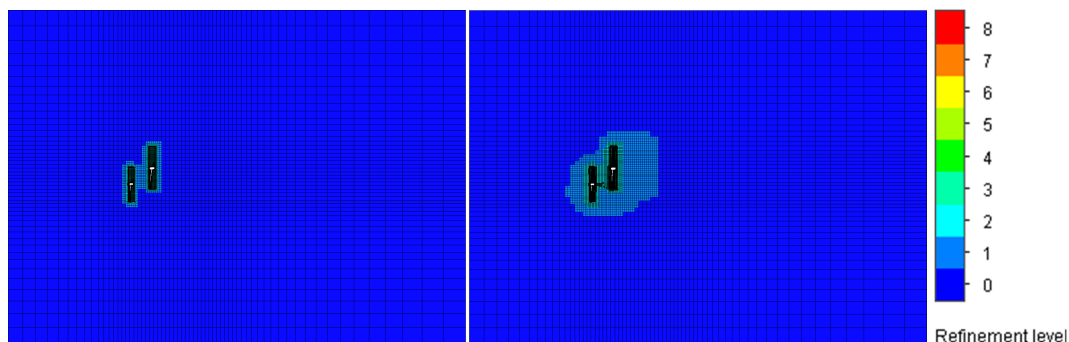


Figure 14. Initial and final mesh for $D_2/D_1 = 1.25$ case (side view, whole domain)

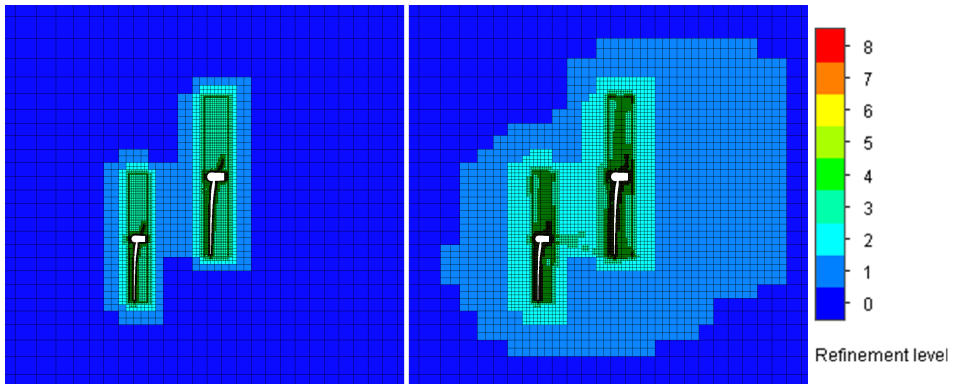


Figure 15. Initial and final mesh for $D_2/D_1 = 1.25$ case (side view, zoom 1)

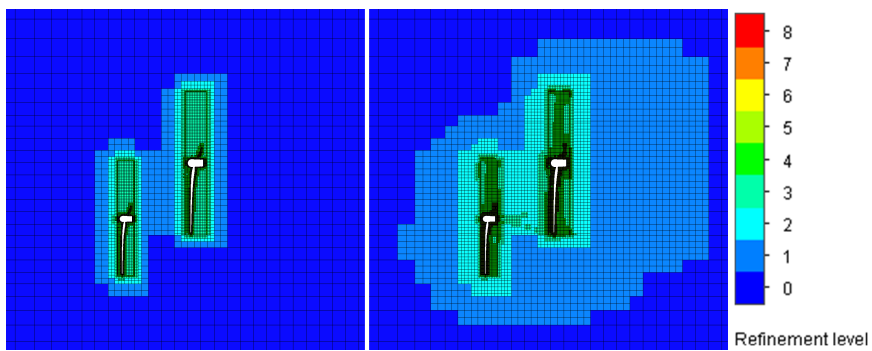


Figure 16. Initial and final mesh for $D_2/D_1 = 1.25$ case (side view, zoom 2)

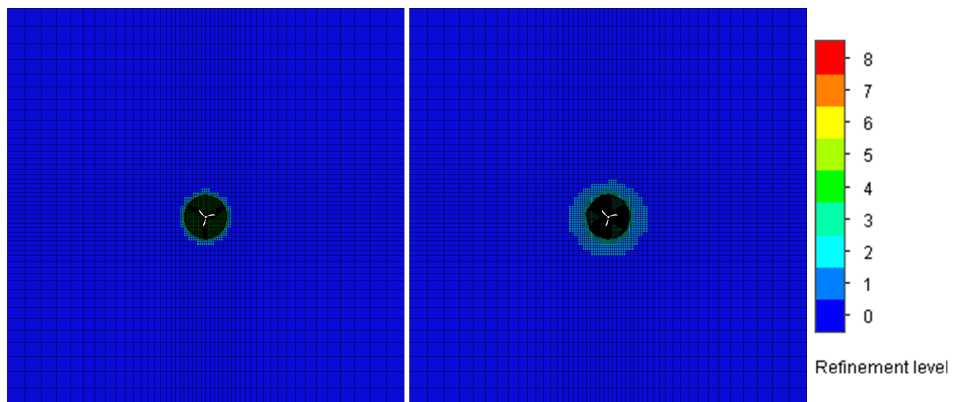


Figure 17. Initial and final mesh for $D_2/D_1 = 1.25$ case (front view, whole domain)

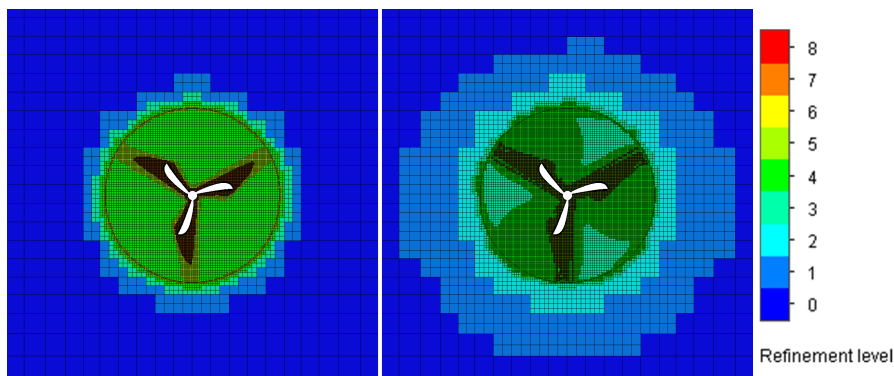


Figure 18. Initial and final mesh for $D_2/D_1 = 1.25$ case (front view, zoom 1)

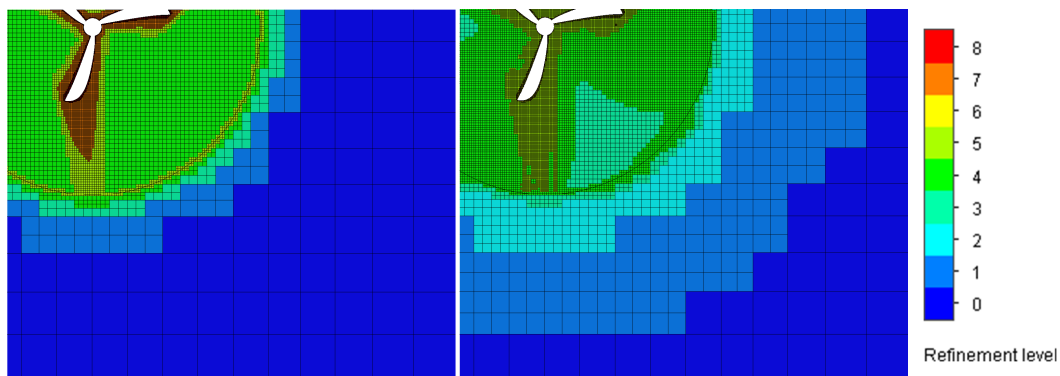


Figure 19. Initial and final mesh for $D_2/D_1 = 1.25$ case (front view, zoom 2)

RESULTS

The flow field was similar for each analysed case. Downstream the turbines, the velocities are generally lower than in the free flow region, as energy is extracted from the wind. The local velocities are higher near the wing's tip, where the vortex shedding can be observed. The velocity distribution in the wake region of the turbines is shown in Figure 20.

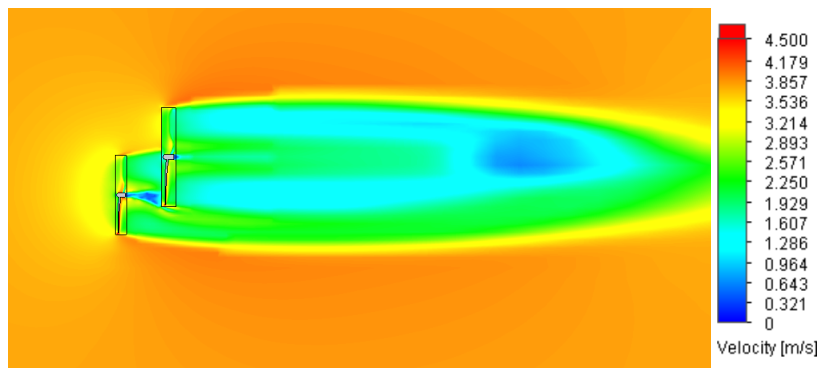


Figure 20. Velocity field near the turbines' region for the $D_2/D_1 = 1.25$ case

The generated torque on the blades' surface was observed in each simulation. As we expected, with the increase of the turbine's diameter the torque increases as well. This tendency is shown in Figure 21.

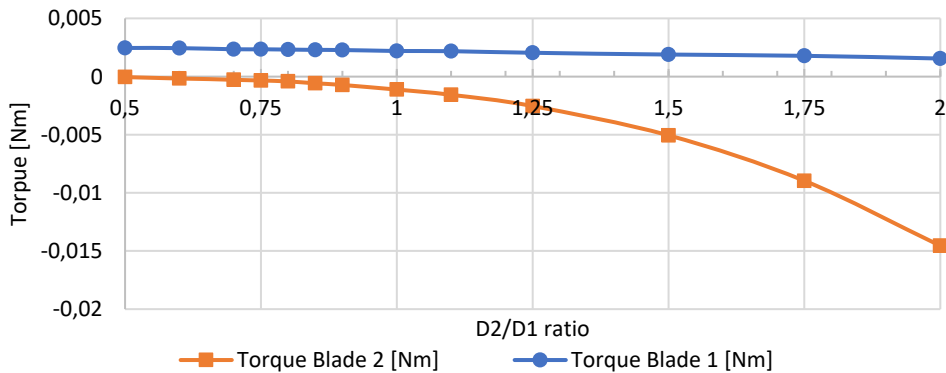


Figure 21. Generated torque by the D_2/D_1 ratio

Using the equation (5) with the flow field's parameters, the swept areas (A_1 and A_2), the torque values (M_1 and M_2), and the angular velocities (ω_1 and ω_2), we were able to establish the power coefficient for each turbine (c_{p1} and c_{p2}). By adding the two coefficient the overall c_p of the CO-DRWT was determined. Selecting the $D_2/D_1=1$ case as a reference point, the c_p 's and the swept areas values compared to the reference study shown in Figure 22.

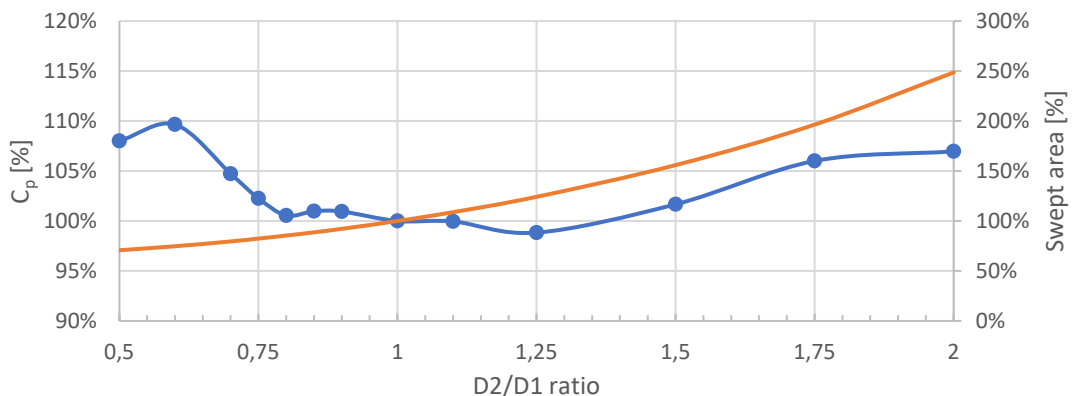


Figure 22. C_p values and the swept area compared to the D_2/D_1 case

Based on the results, the followings can be stated:

1. The first rotor's torque decreased almost linearly. For the 0.5 diameter ratio, the torque was 111.4% of the torque of the $D_2/D_1=1$ case, for the $D_2/D_1=2$ ratio the torque was 70.5% of the comparison base.
2. The second turbine's torque was increased exponentially from 3.5% to 1306.3% compared to the $D_2/D_1=1$ case.
3. The overall torque was constantly growing with the increase of the second turbine's size.

4. The overall c_p 's maximum was 109.66% at $D_2/D_1=0.6$, the minimum was 98.84% at $D_2/D_1=1.25$ (compared to the $D_2/D_1=1$ case).
5. The change of overall c_p 's function started with a jump from 108% to 109.66% and then decreased until the $D_2/D_1=1.25$ case from where it is increased to the end.
6. Higher power coefficient for the CO-DRWT than the $D_2/D_1=1$ case was reached on both ends of the examined interval.
7. The difference between measured (which was described in chapter *Measurement method*) and the simulated c_p was 25.02%.
8. The measured c_p was higher than the simulated.

The 6th conclusion shown similarity with the turbines concept of Rosenberg *et al.* [20], who analysed a dual rotor wind turbine where the rotors were co-axial.

The 7th conclusion (the difference between the measured and simulated c_p) presumed cause is the geometric differences, e.g. the tower, ground, and surface roughness.

CONCLUSIONS

In the presented study we analysed a CO-DRWT (counter-rotating dual-rotor wind turbine), where the second turbine's diameter was varied, and the dual-rotor configurations had a constant axial and radial gap. The analysis was carried out with a CFD software and the overall power coefficient of the CO-DRWT was plotted against the change of the diameter ratio (Figure 22).

Based on the measurements of Ozbay *et al.* [15], we know the CO-DRWTs are more efficient than the co-rotating dual-rotor wind turbines and the single rotor wind turbines. According to the presented study, the change of the turbine size can increase (and decrease) the CO-DRWT's overall power coefficient (c_p) in the same way it is affected by changing the distance [21]. Due to the possible growth of the overall c_p , a wisely chosen CO-DRWT configurations can increase a wind farm energy density which will help increase the energy security of the area's population and can reduce the share of non-renewable energy sources.

BIBLIOGRAPHY

- [1] Szlivka Ferenc, Molnár Ildikó, "Víz- és szélenergia hasznosítás (*Hydro and wind energy utilization*)", Edutus Főiskola Kiadó, 2012, https://regi.tankonyvtar.hu/hu/tartalom/tamop412A/2010-0017_10_viz_es_szelenergia/index.html
- [2] Nashtifan Windmills, <http://historicaliran.blogspot.hu/2012/03/nashtifan-wind-mills.html> (Access Date: 23. 09. 2019.)
- [3] Miles Kelly, "Cross-Section of Wooden Windmill", <https://gb.fotolibra.com/images/previews/49532-cross-section-of-wooden-windmill-illustration.jpeg> (Access Date: 11. 05. 2020.)
- [4] "Windmill", <https://en.wikipedia.org/wiki/Windmill> (Access Date: 23. 04. 2020.)
- [5] "Blyth's Wind Turbine", https://upload.wikimedia.org/wikipedia/commons/1/13/James_Blyth%27s_1891_windmill.jpg (Access Date: 23. 04. 2020.)
- [6] "Charles F. Brush Wind Turbine", <https://media2.fdncoms.com/clevescene/imaget/tilting-at-windmills/u/zoom/2622441/cover-3.jpg> (Access Date: 23. 04. 2020.)

- [7] BP, “*Statistical Review of World Energy*”, BP Statistical Review of World Energy, London (UK), p. 50, 2019, <https://www.bp.com/content/dam/bp/business-sites/en/global/corporate/pdfs/energy-economics/statistical-review/bp-stats-review-2019-full-report.pdf>
- [8] Canadian Wind Energy Association, “*Small Wind Siting and Zoning - Study Development Of Siting Guidelines And A Model Zoning By-Law For Small Wind Turbines (Under 300 kW)*”, 2006, p. 3. http://www.toolkit.bc.ca/sites/default/files/Small_Wind_Siting_Bylaw%20and%20Guidelines.pdf (2020.05.28.)
- [9] “*Wind Turbines on the roof*”, <https://i.ytimg.com/vi/ECjAj23GkLQ/maxresdefault.jpg> (Access Date: 29. 03. 2020.)
- [10] “*Mini wind turbine and solar cell on a street light pole. - cca 11 Istenhegyi út Budapest District XII., Hungary*”, https://upload.wikimedia.org/wikipedia/commons/6/6c/Wind_turbine_and_solar_cell_on_a_street_light_pole._-Istenhegyi_%C3%BAt%2C_Budapest_XII.JPG (Access Date: 29. 03. 2020.)
- [11] “*ENLIL Vertical Axis Wind Turbine on the street of Istanbul*”, <http://okosvaros.lechnerkozpont.hu/en/node/703> (Access Date: 29. 03. 2020.)
- [12] Romańsk L. et al., “*Estimation of operational parameters of the counter-rotating wind turbine with artificial neural networks*”, Archives of Civil and Mechanical Engineering, 17(4), pp. 1019-1028, 2017, <https://10.1016/j.acme.2017.04.010>
- [13] “*Unconventional Wind Turbines*”, <http://www.whirlopedia.com/images/wind-turbines-elk.jpg> (Access Date: 23. 04. 2020.)
- [14] “*Bizarre Wind Turbines*”, <https://cdn.trendhunterstatic.com/thumbs/urban-wind-turbine.jpeg> (Access Date: 29. 03. 2020.)
- [15] Ozbay A., Tian W., Hu H., “*Experimental Investigation on the Wake Characteristics and Aeromechanics of Dual-Rotor Wind Turbines*”, Journal of Engineering for Gas Turbines and Power, 138(4), pp. 1-15, 2016, <https://doi.org/10.1115/1.4031476>
- [16] Lee S., Kim H., Son E., Lee S., “*Effects of design parameters on aerodynamic*”, Renewable Energy, 42(1), pp. 140-144, 2012, <https://doi.org/10.1016/j.renene.2011.08.046>
- [17] Gorban A. N., Gorlov A. M., Silantyev V. M., “*Limits of the Turbine Efficiency for Free Fluid Flow*”, Journal of Energy Resources Technology, 123(4), pp. 311-317, 2001, <https://doi.org/10.1115/1.1414137>
- [18] Kristóf G., “*Áramlások numerikus modellezése (Numerical modelling of flows)*”, Akadémia Kiadó, Budapest, 2019., ISBN 978-963-454-412-8, <https://doi.org/10.1556/9789634544128>
- [19] Szlivka F., Molnár I., Kajtár P., Telekes G., “*CFX Simulations by Twin Wind Turbine*”, 2011 International Conference on Electrical and Control Engineering, 2011, Yichang, China, 16-18 Sept. 2011 pp. 5780 – 5783, <https://doi.org/10.1109/ICECENG.2011.6057550>
- [20] Rosenberg A., Selvaraj S., Sharma A., “*A Novel Dual-Rotor Turbine for Increased Wind Energy Capture*”, Journal of Physics Conference Series, 524(1), 2014, 18–20 June 2014, Copenhagen, Denmark, <https://doi.org/10.1088/1742-6596/524/1/012078>
- [21] Heteyei Cs. and Szlivka F., “*Axial Gap Optimisation of Half Diameter Shifted Counter Rotating Dual Rotor Wind Turbine*”, Interdisciplinary Description of Complex Systems, 18(3), pp. 389-399, 2020, <https://doi.org/10.7906/indecs.18.3.9>